Acoustic bound states in the continuum in coupled Helmholtz resonators

Mariia Krasikova,[1,2,*] Felix Kronowetter,[2,‡] Sergey Krasikov,[1,‡] Mikhail Kuzmin,[1] Marcus Maeder,[2] Tao Yang,[2] Anton Melnikov,[2] Steffen Marburg,[2] and Andrey Bogdanov[1,3,†]

[1] *School of Physics and Engineering, ITMO University, St. Petersburg 197101, Russia*

[2] *Chair of Vibroacoustics of Vehicles and Machines, Technical University of Munich, Garching b. München 85748, Germany*

[3] *Qingdao Innovation and Development Center, Harbin Engineering University, Qingdao 266000, Shandong, China*

(Received 12 May 2024; revised 13 July 2024; accepted 30 July 2024; published 15 August 2024)

Resonant states underpin a variety of metastructures that exhibit remarkable capabilities for the effective control of acoustic waves at subwavelength scales. The development of metamaterials relies on rigorous mode engineering, providing the implementation of the desired properties. At the same time, the application of metamaterials is still limited, as their building blocks are frequently characterized by complicated geometry and cannot be tuned easily. In this work, we consider a simple system of coupled Helmholtz resonators and study their properties associated with the tuning of coupling strength and symmetry breaking. We numerically and experimentally demonstrate the excitation of the quasibound state in the continuum in the resonators placed in free space and in a rectangular cavity. It is also shown that tuning the intrinsic losses via introducing porous inserts can lead to spectral splitting or merging of *quasibound states in the continuum* and the occurrence of *exceptional points*. The obtained results open opportunities for the development of simple and easily tunable metastructures based on Helmholtz resonances.

DOI: 10.1103/PhysRevApplied.22.024045

I. INTRODUCTION

Acoustic resonances play a pivotal role in a variety of practical applications, covering all aspects of modern society, including art and entertainment [1–3], medicine [4–6], industrial applications [7,8], and even cosmology [9]. The importance of resonances has become more prominent with the rise of metamaterials [10–12], allowing effective control over acoustic fields at the subwavelength scale. Remarkable properties such as negative mass density [13,14], hyperlensing [15], or subwavelength perfect absorption [16] arise from the resonant states and the interplay between them. Further progress in the field of metamaterials nowadays is associated with resonant-state engineering, involving concepts such as topological states [17,18], nonlocality [19], and symmetry breaking [20].

Of particular interest in this case are the so-called *bound states in the continuum* [21,22] (BIC), also known previously as trapped waves, which are characterized by infinitely large radiative quality factors and the associated decoupling from the far field, usually originating from the interference of several leaky modes. Historically proposed in the field of quantum mechanics [23], BIC nowadays are actively studied in a variety of other systems, including electrical circuits [24], photonics [22,25], and acoustics [26]. For instance, BIC can be utilized for sound confinement [27,28], acoustic radiation enhancement [29], or improvement of noise-insulating systems [30,31]. Acoustic BIC were also studied in pipe and duct-cavity systems [32,33], as well as in various configurations of single and coupled resonators [34–37] and elastic systems [38–41]. Since genuine BIC cannot be excited from the far field due to decoupling, practical applications utilize the so-called quasi-BIC, which have a large but finite radiative quality factor. The excitation of quasi-BIC is associated with symmetry breaking, which allows weak coupling with the far field [42].

Symmetry breaking plays a key role not only in the engineering of high-Q quasi-BICs but also in bianisotropic [43–47] and non-Hermitian systems [19,29,48]. In particular, the *exceptional point* (EP), which denotes a condition where two or more eigenmodes and their complex eigenfrequencies coalesce, is achieved via breaking of parity (P symmetry) and time-reversal symmetry (T symmetry) [49–51]. Today, EPs find a variety of applications in photonics and acoustics [29,52]. Practical implementations of EPs in acoustic systems have enabled asymmetric field

*Contact author: mariia.krasikova@metalab.ifmo.ru

†Contact author: a.bogdanov@metalab.ifmo.ru

‡F. Kronowetter and S. Krasikov contributed equally to this work.

propagation [53], mode stabilization [54], and enhanced absorption [55].

Therefore, it can be inferred that singularities such as BIC and EPs are pivotal for the engineering of acoustic metamaterials and devices with unique functionality and performance. However, their practical implementations are still limited by the typically nontrivial geometry of unit cells and the narrow operational frequency range. Producing metastructures with easily tunable designs and acoustic properties is also a difficult task, which sometimes requires the use of nontrivial algorithms of numerical optimization. Therefore, the creation of resonant meta-atoms with straightforward designs that facilitate the easy adjustment of resonant and singular states, including BIC and EPs, could greatly enhance the adoption of metamaterials in real-world applications.

In this study, we suggest and explore the straightforward design of a meta-atom with easily tuned acoustic properties. The suggested meta-atom represents a pair of two-dimensional coupled C-shaped Helmholtz resonators. Such a system can be tuned via mechanical displacement of the resonators from each other, as well as via the adjustment of their intrinsic losses using absorbing inserts made of conventional porous materials. We demonstrate experimentally that such a meta-atom supports quasi-BIC that could be merged into an EP via the tuning of intrinsic losses.

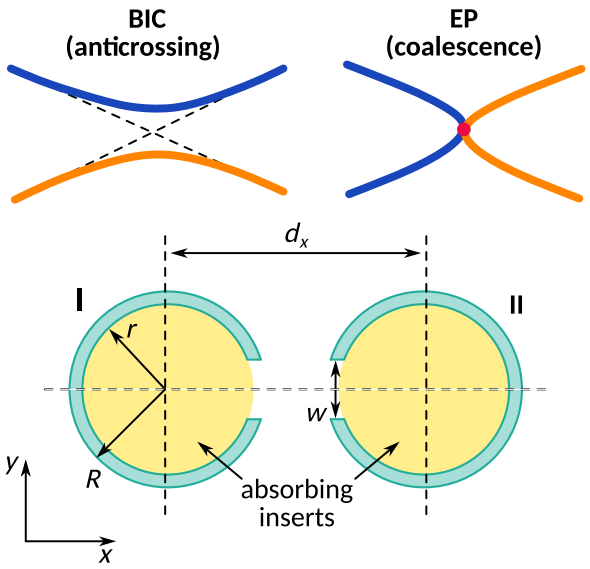

FIG. 1. Illustration of the working concept. BIC occur at the anticrossings formed by real parts of symmetric and antisymmetric modes in parametric space. EP represents a special case of a coupling regime when the eigenmodes coalesce in the real and imaginary planes. In the considered system of two coupled Helmholtz resonators, these regimes can be achieved by tuning the distance between the resonators and tuning their intrinsic losses. Both of the resonators are characterized by the inner radius, r; the outer radius, R; and the slit width, w. In addition, the volume of the resonators is supplemented by absorbing inserts.

II. METHODS

A. System description

The considered system consists of coupled two-dimensional (2D) Helmholtz resonators with circular cross sections, as shown in Fig. 1. The coupling can be tuned via the change of distance between the resonators and their mutual orientation, while the intrinsic losses can be controlled by absorbing inserts. Resonators of similar shapes were considered, for instance, in Refs. [45,56–59]. Normal modes of such a system are formed by the superposition of the modes of solitary resonators. In-phase excitation of the resonators corresponds to a symmetric mode, which in optics is usually called a bright one, since it can be directly excited and observed from the far field. On the other hand, the resonators can be excited out of phase, forming an antisymmetric mode.

When an antisymmetric mode is localized entirely inside the resonators, its radiative quality factor is infinite. Such states are genuine BIC, the coupling of which with the far field is prohibited for symmetry reasons. Therefore, the excitation of BIC implies symmetry breaking, allowing the transformation of BIC into quasi-BIC, the radiative quality factor of which is still large but finite. Regarding eigenmodes, BIC occur in the strong mode-coupling regime when the dispersion curves (real parts of eigenfrequencies) are repelled. For weak coupling, the situation is reversed and the real parts of modes are crossed. In between these regimes, an EP can be achieved in which both real and imaginary parts of the modes coalesce and the eigenmodes become linearly dependent. In the considered system, the coupling between the modes can be easily tuned via simple displacement of the resonators, affecting the radiative losses. At the same time, the intrinsic losses and coupling between the resonators can be tuned via the introduction of porous inserts into their volume. Hence, it might be expected that a simple variation of several parameters is enough to achieve the considered coupling regimes.

B. Numerical calculations

All numerical calculations are performed in COMSOL Multiphysics using the "pressure acoustics" physics feature. The incident plane wave is introduced as the background-pressure field with an amplitude of $p_0 = 1$ Pa. The pressure inside the resonators is defined as a root mean square of pressure calculated at several sampling points located inside the resonators. To account for thermoviscous dissipation in the boundary layer of the resonators' walls, the "thermoviscous boundary layer impedance" condition is applied to the corresponding boundaries. Porous inserts are included via the "poroacoustics" feature utilizing the Delany-Bazley-Miki model.

For the case of the transmission tube, the three-dimensional (3D) model is considered, in which the transmission coefficient is calculated as the amplitude of the total pressure over the corresponding background pressure, i.e.,

$$T = \frac{P_t}{P_b}, \tag{1}$$

such that the pressure amplitudes are averaged over a small volume in the transmission zone of the structure:

$$P_{t,b} = \frac{1}{V}\int_V |p_{t,b}|^2 dV. \tag{2}$$

The corresponding transmission-loss coefficient is then obtained as

$$T_L = 10\log_{10}(1/T). \tag{3}$$

C. Experimental measurements

For the resonators placed in free space, the measurements are performed in the 2D anechoic chamber, representing a waveguide with walls covered by absorbing mineral wood [see Figs. 2(a) and 2(b)]. In particular, the walls and bottom of the waveguide are made of 15-mm-thick aluminum plates, and the lid is made of 6-mm-thick plexiglass. Since the impedance contrast between air and most of the solid materials is huge [60], the lid and the bottom can be considered as sound-hard walls. The height of the waveguide is 60 mm, while the width and the length are 650 and 1350 mm, respectively. The thickness of the mineral-wood inserts is 300 mm (from a wall to the tip of a pyramid). Generation and recording of the sound signal is done using the Crysound CRY6151B analysis system and the 1/4" Crysound CRY342 pressure-field microphone. To mitigate the influence of random noise, the signal is

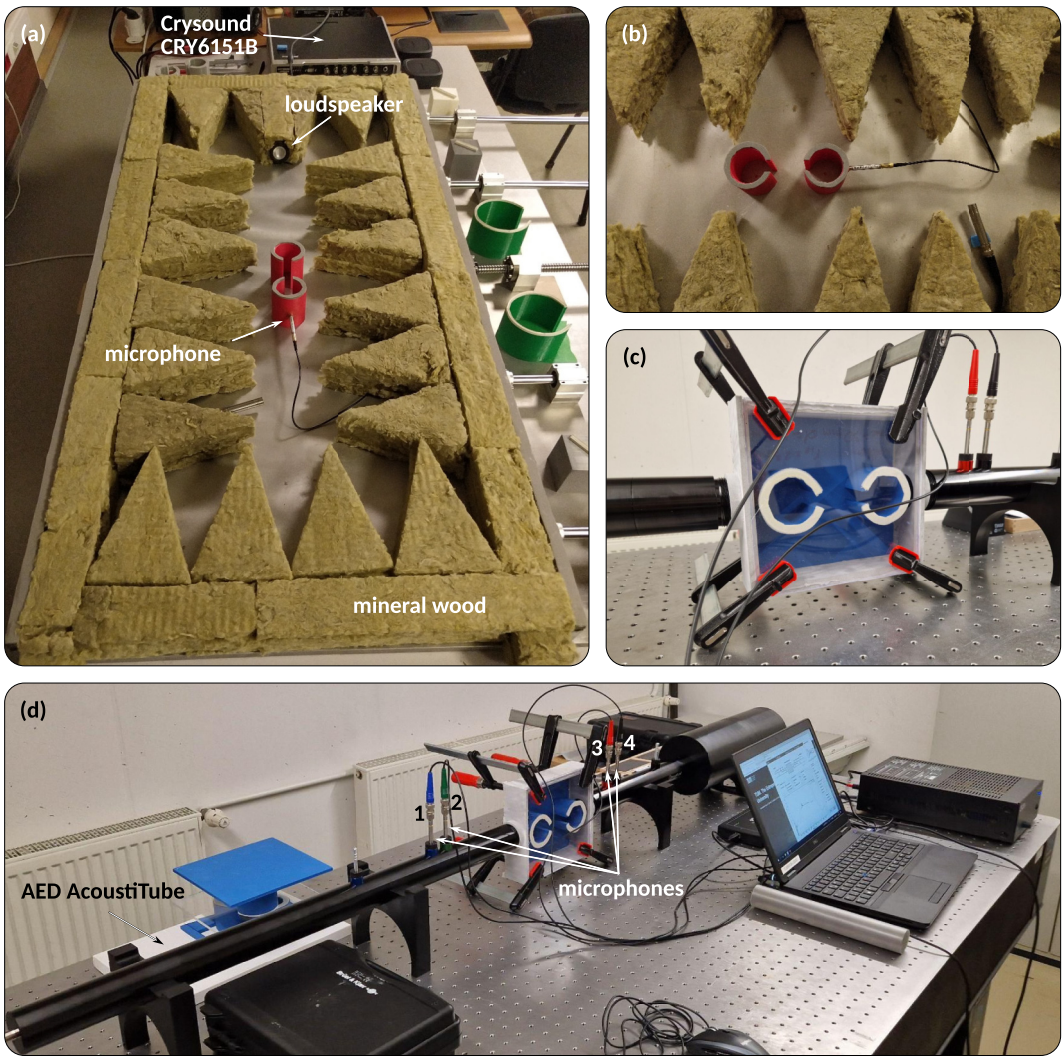

FIG. 2. Experimental setups and samples. (a) Photograph of the 2D anechoic chamber imitating free space. Close up photographs of (b) samples used in the 2D anechoic chamber and (c) samples and the box used for transmission-tube measurements. (d) Photograph of the transmission-tube setup.

recorded several times and then averaged in the Fourier domain.

The transmission-loss measurements are conducted in the AED AcoustiTube measurement system, the impedance tube. In this case, the resonators are placed in a box with a rectangular cross section [see Figs. 2(c) and 2(d)]. The width of the box is 170 mm, the height is 160 mm, and the thickness is 40 mm. The scattering coefficients are extracted from the measured T-matrix coefficients using conventional expressions [61]:

$$t^{-} = \frac{2e^{ikL}}{T_{11} + T_{12}/Z_L + T_{21}Z_0 + T_2 2Z_0/Z_L}, \tag{4}$$

$$t^{+} = \frac{Z_0}{Z_L}\frac{2e^{ikL}(T_{11}T_{22} - T_{12}T_{21})}{T_{11} + T_{12}/Z_L + T_{21}Z_0 + T_2 2Z_0/Z_L}, \tag{5}$$

$$r^{-} = \frac{T_{11} + T_{12}/Z_L - T_{21}Z_0 - T_2 2Z_0/Z_L}{T_{11} + T_{12}/Z_L + T_{21}Z_0 + T_2 2Z_0/Z_L}, \tag{6}$$

$$r^{+} = \frac{-T_{11} + T_{12}/Z_L - T_{21}Z_0 + T_2 2Z_0/Z_L}{T_{11} + T_{12}/Z_L + T_{21}Z_0 + T_2 2Z_0/Z_L}, \tag{7}$$

where Z_0 and Z_L are acoustic impedances of the media at the sides of the structure, such that L is the thickness of the structure, and the superscripts indicate the positive (+) and (−) negative directions of incident-wave propagation. The amplitude coefficients can then be defined as $T^{+,-} = |t^{+,-}|^2$ and $R^{+,-} = |r^{+,-}|^2$. Correspondingly, the absorption coefficients can be defined as $A^{+,-} = 1 - |r^{+,-}|^2 - |t^{+,-}|^2$. When the system is symmetric, $R = R^{+} = R^{-}$, $T = T^{+} = T^{-}$, and $A = A^{+} = A^{-}$. Note that all measured spectra are slightly smoothed using the third-order Savitzky-Golay filter and with a window width of 11.

All resonators are fabricated by 3D printing using the well-known fused-deposition modeling technology, for which polylactic acid is used as a filament. In the case of 2D anechoic chamber measurements, the resonators are manufactured on a Creality K1 3D printer (Shenzhen Creality 3D Technology Co., Ltd., Shenzhen, China). For the impedance-tube measurements, a Bambu Lab X1-Carbon 3D printer (Shenzhen Tuozhu Technology Co., Ltd., Shenzhen, China) is used to produce the resonators. Typical 0.4-mm nozzles, and standard slicing settings are used for both 3D printers to achieve the sample resolution of approximately 0.2 mm. To avoid gaps between the resonators and the lids, the tops of the resonators are supplemented by thin porous inserts.

The quality factors of quasi-BIC are estimated from the spectral curves as the ratio of the center frequency to the −3-dB bandwidth:

$$Q = \frac{f_0}{\Delta f_{-3\,\mathrm{dB}}}. \tag{8}$$

The central frequency, f_0, is determined programmatically as the frequency at which the maximum of the peak is located. The value of amplitude at f_0 is considered as y_0, and the bandwidth is determined as the difference of frequencies at which the resonance-curve intersects the y_0-−3-dB line (the corresponding sketch is provided in the Supplemental Material [62]). Note that for the case of $d_x = 70$ mm, the peak is not pronounced and there is only one intersection of the resonance curve and the y_0-−3-dB line. Hence, this particular resonance curve is fitted using a Lorentzian function, and the bandwidth is calculated for this fitting curve.

III. RESULTS

A. Quasi-BIC

1. Numerical simulations

The considerations start with the resonators without absorbing inserts. For this case, the geometric parameters of the resonators are fixed to have an outer radius of the resonators of $R = 30$ mm, an inner radius of $r = 23$ mm, and a slit width of $w = 14$ mm, which correspond to the scaled geometry considered in Refs. [58,59]. At first, the resonators placed in free space are considered [see Fig. 3(a)]. Such a system is characterized by two eigenmodes with symmetric and antisymmetric field distributions [Fig. 3(b)], which correspond to the resonances of pressure spectra inside one of the resonators [Fig. 3(c)]. When the distance between the resonators becomes large enough, they almost do not interact and their eigenfrequencies become almost identical, corresponding to the frequency of a single Helmholtz resonator. On the contrary, the spectral width of the mode with the antisymmetric distribution vanishes for small d_x when resonators are close to each other; this is associated with the vanishing of the imaginary parts of eigenmodes [Fig. 3(d)]. Therefore, the real parts of the modes merge with the increase of d_x, demonstrating the independent behavior of two noninteracting resonators, while the imaginary parts diverge and vice versa. This is a manifestation of symmetry-protected quasi-BIC, which become genuine BIC when the imaginary part of the mode is equal to zero.

2. Anechoic chamber measurements

The numerical calculations are verified by the measurement of pressure inside the resonators placed in the 2D anechoic chamber (see Sec. II). As shown in [Fig. 3(e)], quasi-BIC manifest as peaks in the pressure spectra, occurring within the range of 900–1200 Hz, depending on the distance between resonators. For instance, when $d_x =$ 100 mm, quasi-BIC are excited at approximately 1025 Hz, and their estimated Q factor is 88. A comparison of the frequencies and Q factors is provided in Table I, while

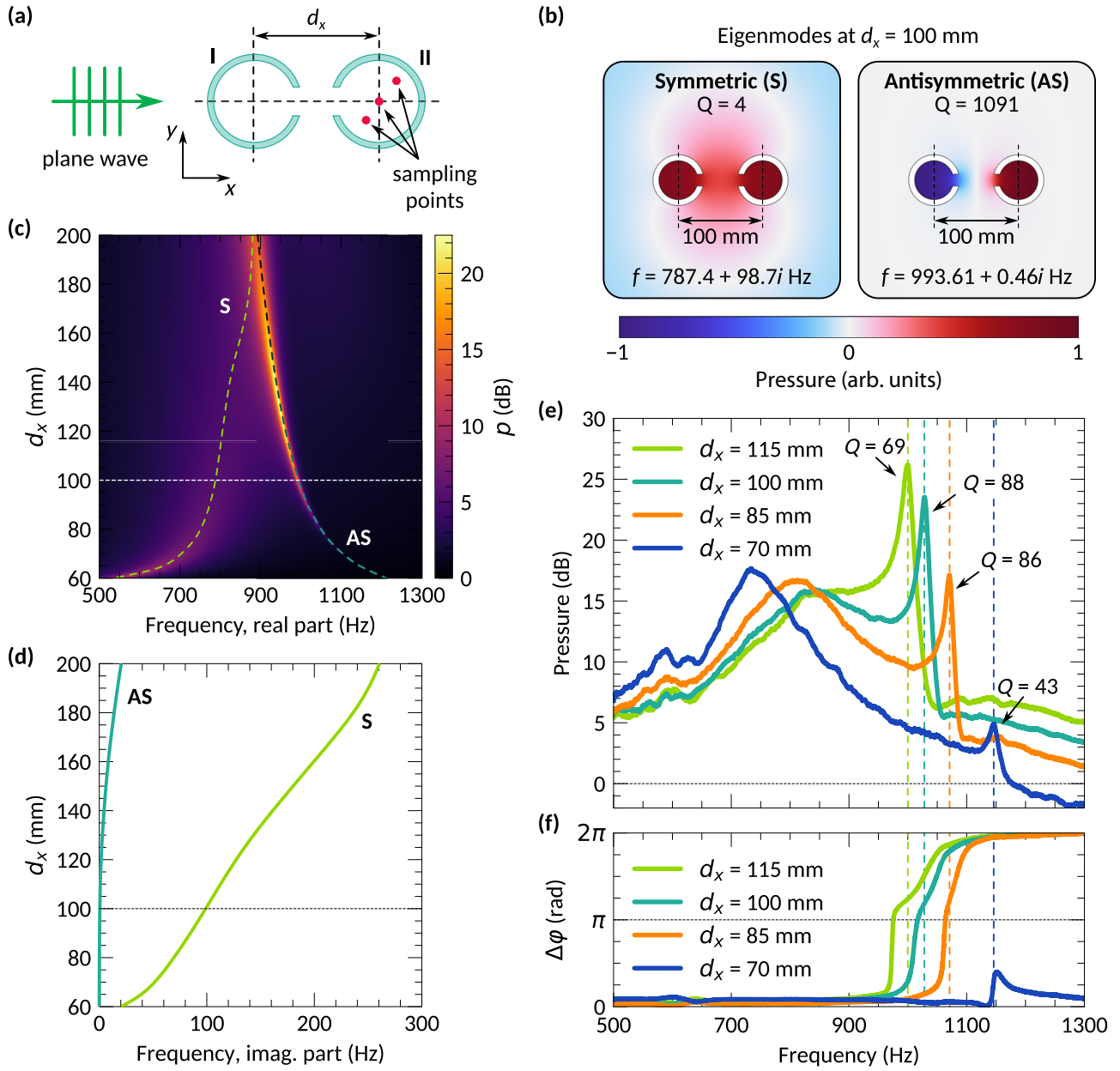

FIG. 3. Quasi-BIC in the resonators placed in free space. (a) Schematic illustration of the considered system. (b) Eigenmode field distributions at $d_x = 100$ mm and their quality factor, Q. (c) Pressure spectra inside one of the resonators as a function of the distance, d_x, between resonators. Dashed lines indicate the corresponding eigenmodes with symmetric (S) and antisymmetric (AS) field distributions. (d) Imaginary part of the eigenfrequencies as a function of d_x. (e) Measured pressure spectra inside one of the resonators. Values of Q indicate the corresponding quality factors of the resonances. (f) Measured spectra of the phase difference between fields inside the resonators.

an explicit comparison of the numerical and experimental spectra is shown in the Supplemental Material [62]. In accordance with the numerical calculations, quasi-BIC shift towards higher frequencies with a decrease in the distance between resonators since the coupling between resonators becomes stronger. At the same time, a decrease in the distance results in a weakening of the coupling with the far field, so the corresponding resonance cannot be excited properly, which means that its amplitude and Q factor are small, as observed for both numerical and experimental results.

By definition, the antisymmetric mode is characterized by the π-phase difference between fields inside the resonators, which can be seen from the spectra in Fig. 3(f), demonstrating conventional smooth steplike shapes. Note that for the case of $d_x = 70$ mm, the phase difference does

TABLE I. Quality factor of quasi-BIC resonances of the system consisting of two coupled resonators placed in free space.

	Frequency (Hz)		Q factor	
d_x (mm)	Num.	Expt.	Num.	Expt.
70	1101	1146	95	43
85	1029	1071	137	86
100	991	1028	131	88
115	967	1000	107	69

not reach the value of π; this might be explained by weak coupling of the antisymmetric mode with the far field.

In addition, it should be noted that the resonances of the measured spectra are shifted from the numerically calculated ones by approximately 30–50 Hz, which arises from manufacturing errors, as submillimeter changes in the resonator sizes affect the position of the resonances (see the Supplemental Material [62]). However, the experimental results are in good agreement with those of numerical simulations. It also should be mentioned that, apart from the geometric parameters, the positions of quasi-BIC are affected by material parameters of the media in which the resonators are placed. Such a property might be promising for the development of devices for the sensing of gaseous and liquid analytes (see the Supplemental Material [62] for an example).

3. Transmission-tube measurements

While the quasi-BIC mode is weakly coupled to the far field, it is also almost decoupled from the other modes of the system. Hence, it can be expected that quasi-BIC can still be excited even if the environment of the resonators changes. For instance, the resonators can be placed inside a rectangular cavity [see Fig. 4(a)], which actually by itself supports quasi-BIC [63]. When the antisymmetric modes of the cavity and the resonators do not interact, the transmission-loss spectra of such a system should also demonstrate a high-Q peak near the frequency corresponding to quasi-BIC occurring for the case of the resonators in free space. Indeed, Fig. 4(b) shows the presence of the two pronounced resonances near 940 and 1000 Hz, obtained via the impedance-tube measurements (see Sec. II). Again, the phase difference between fields inside the resonators represents the smooth steplike curve [see Fig. 4(c)], demonstrating that the phase difference is nearly $\Delta\varphi = \pi$ at the quasi-BIC frequency.

The peak of the transmission-loss spectrum occurring near 940 Hz can be associated with the symmetric excitation of Helmholtz resonators [see Fig. 4(f)], leading to a decrease of the transmission coefficient [Fig. 4(d)]. At the same time, the second peak in the transmission spectra, occurring near 1000 Hz, corresponds to quasi-BIC characterized by the antisymmetric field distribution, as previously [see Fig. 4(f)]. The resonance in the transmission loss, in this case, is related to the increase of the absorption coefficient [see Figs. 4(d) and 4(e)]. However, it should be noted that numerical and experimental results in this case do not perfectly agree with each other. While in both cases there is an absorption peak at the frequency of quasi-BIC, for the experimental curve the absorption is higher, especially at the frequency of the symmetric resonance. Such a difference is associated with energy leakage into the mechanical vibrations of the box walls, which are not taken into account in the numerical calculations. The presence of the box-wall vibrations is verified using the laser Doppler vibrometry technique (Polytec PSV-500-3D), but elimination or analysis of these vibrations lie beyond the scope of the present work.

B. Tuning of intrinsic losses

Apart from the distance between resonators, the resonances can be controlled by introducing porous materials into the volume of the resonators. Such inserts may significantly decrease the quality factor of a standalone Helmholtz resonator (see the Supplemental Material [62]), practically leading to the destruction of the resonance. At the same time, the introduction of intrinsic losses may result in inversion-symmetry breakage and the associated asymmetric absorption (see the Supplemental Material [62]). Small intrinsic losses can be used for the fine-tuning of quasi-BIC. For instance, the system supplemented with an additional pair of resonators can be considered, such that this additional pair is supplemented by absorbing inserts made of a porous material with a flow resistivity of R_{f_2}, while another pair has no such inserts [see Fig. 5(a)]. Since there are four resonators in such a system, it is characterized by four eigenmodes [see Fig. 5(b)], two of which are characterized by the symmetric field distributions within the pairs and two by the antisymmetric field [see Fig. 5(c)]. When the flow resistivity, R_{f_2}, is zero, the antisymmetric eigenmodes are nearly degenerate, which means that they have equal real parts of the frequencies, but slightly different values for the imaginary parts. Both the real and imaginary parts of the symmetric modes are almost not affected by the change of R_{f_2}. At the same time, the increase of R_{f_2} results in the splitting of quasi-BIC [see Figs. 5(b) and 5(c)], such that the frequency of one antisymmetric eigenmode remains the same, while another antisymmetric eigenmode shifts towards smaller real frequencies, while its quality factor quickly decreases. Similar behavior can also be observed experimentally. In this case, the spectral positions of quasi-BIC measured in the first pair remain nearly unchanged [see Fig. 5(e)], while quasi-BIC measured in the second pair shift towards lower frequencies with an increase of the absorbing insert size [see Fig. 5(d)]. These results indicate that the spectral positions of BIC in arrays of Helmholtz resonators can

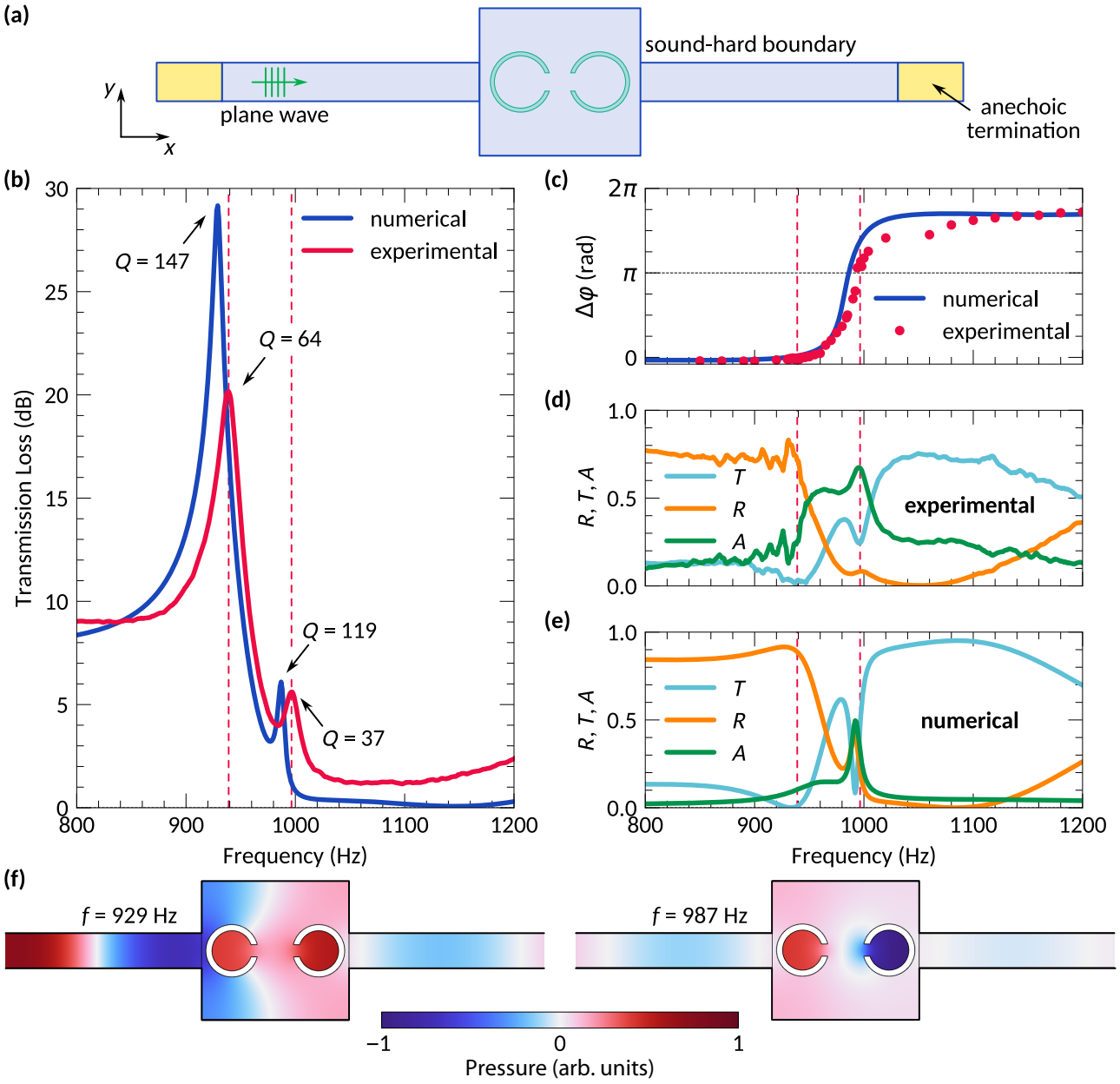

FIG. 4. Transmission-tube measurements of quasi-BIC. (a) Schematic illustration of the system consisting of a box with resonators embedded into the transmission tube. (b) Transmission-loss spectra. (c) Experimentally measured and numerically calculated spectra of the phase difference between fields inside the resonators. (d) Experimentally obtained and (e) numerically calculated reflection, transmission, and absorption coefficients. (f) Field distributions corresponding to transmission-loss resonances occurring near 929 and 987 Hz.

be fine-tuned via simple adjustment of the intrinsic losses controlled by the size of the absorbing inserts.

An important remark is that in the numerical calculations, the insert occupies the whole volume of the resonator, and the corresponding porous material is only characterized by the flow resistivity, which varies. For experimental verification, it is assumed that a small piece of porous material with a large flow resistivity is roughly equivalent to a large piece of a material with a low flow resistivity. In such an approximation, a porous insert occupying the whole volume of the resonator can be represented by an insert occupying only part of the volume [see Fig. 5(d)], and it is much easier to control the size of an insert contrary to its material parameters.

To push the concept further, it should be mentioned that two quasi-BIC can be merged into an EP [64]. Strictly speaking, an EP is characterized by the coalescence of eigenmodes rather than their degeneracy [49],

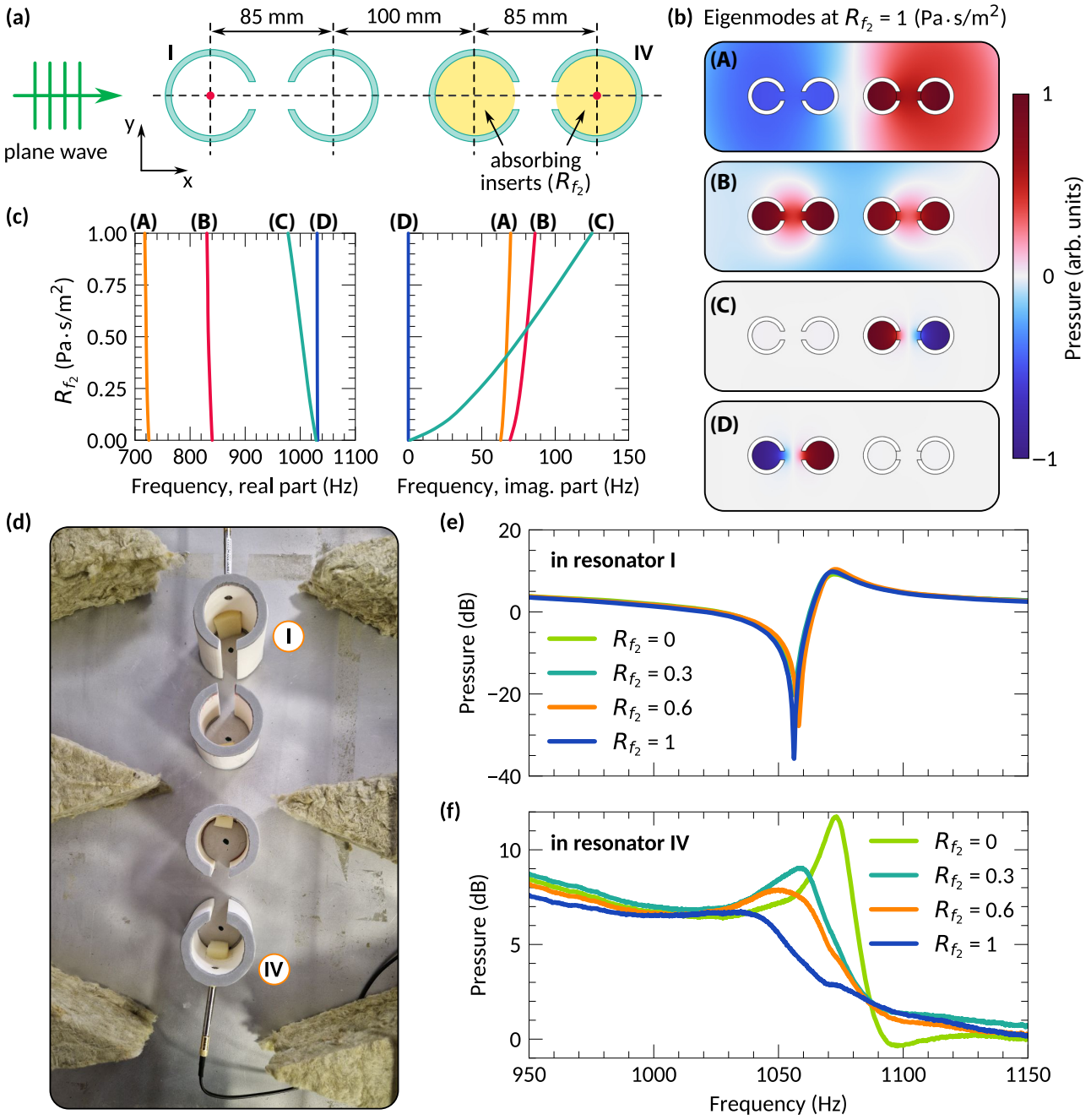

FIG. 5. Splitting of quasi-BIC. (a) Schematic illustration of the considered system, consisting of two pairs of coupled resonators placed in free space. One of the pairs is supplemented by porous inserts with a flow resistivity of R_{f_2}. (b) Eigenmode field distributions for the case of $R_{f_2} = 1$ Pa s/m^2, and (c) real and imaginary parts of eigenmodes for different values of R_{f_2}. (d) Photograph of the samples. Experimentally obtained pressure spectra measured inside (e) resonator I and (f) resonator IV.

which implies intersection of both real and imaginary parts of the eigenmodes in parametric space. This condition can be achieved via fine-tuning of intrinsic losses of the resonators and their coupling [65]. For this, again, absorbing inserts can be used, such that in the first pair, the inserts are characterized by the flow resistivity, R_{f_1}, and in the second pair by R_{f_2} [see Fig. 6(a)]. When losses of the first pair are fixed, the corresponding quasi-BIC excited in the first pair remain unchanged [see Figs. 6(b) and 6(c)]. The change of R_{f_2}, however, results in the deformation of quasi-BIC formed in the second pair, such that their frequencies shift towards lower frequency [see Figs. 6(d) and 6(e)]. At some point, resonances occurring in the first and second pairs become spectrally overlapped, which might indicate the presence of an EP. Indeed, fine-tuning of intrinsic losses and the coupling between resonators results in the spectral

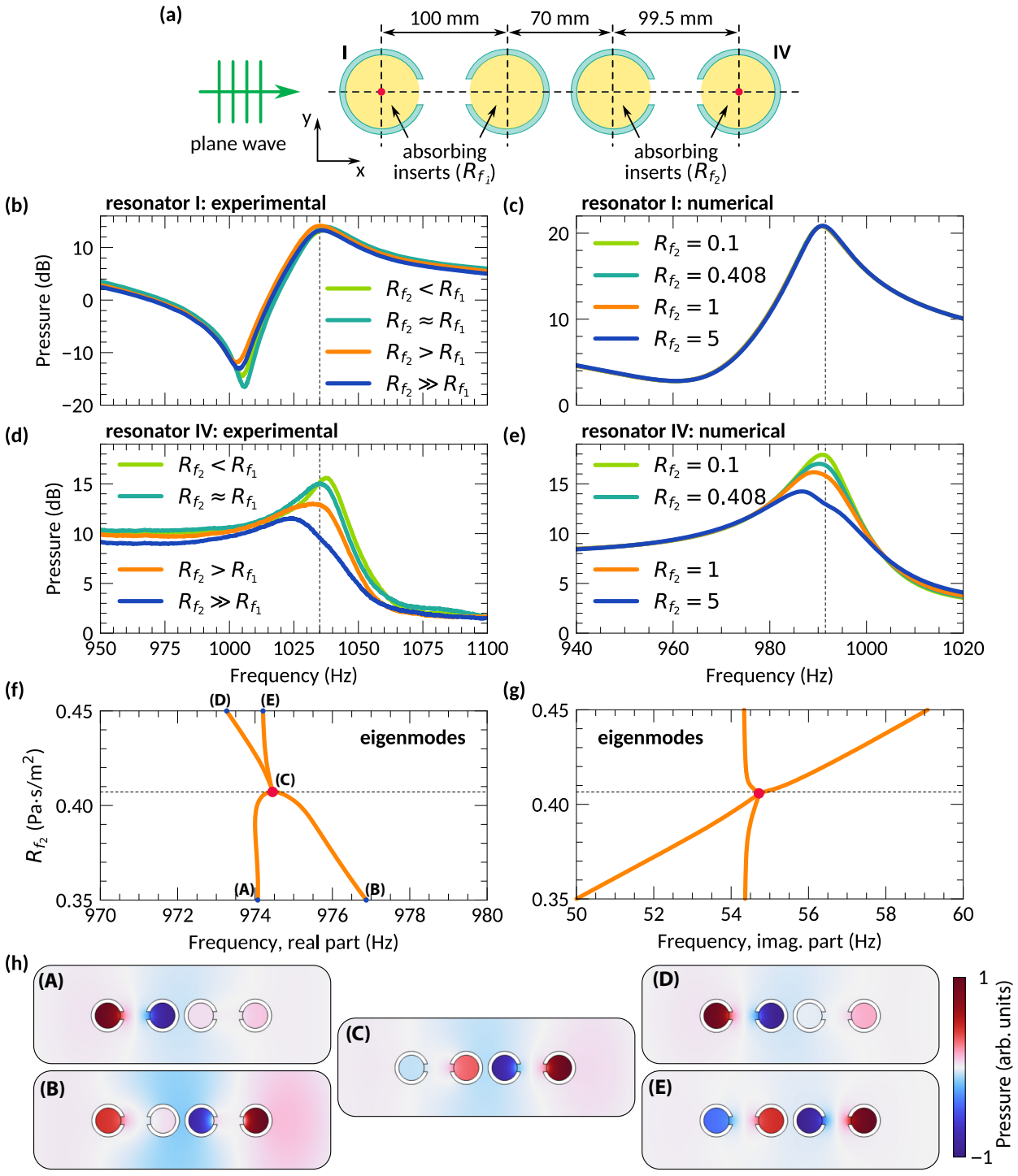

FIG. 6. EP in the system of four resonators. (a) Schematic illustration of the considered system, consisting of two pairs of coupled resonators, both supplemented by porous inserts with flow resistivities of R_{f_1} and R_{f_2}. Pressure spectra experimentally measured inside (b) resonator I and (d) resonator IV, and the corresponding spectra numerically calculated inside (c) resonator I and (e) resonator IV (sampling points are shown by red dots). All numerical results are obtained for $R_{f_1} = 0.4$ Pa s/m^2. (f) Real and (g) imaginary parts of eigenmodes for different values of R_{f_2}, and (h) corresponding field distributions.

merging of two eigenmodes in both real and imaginary spaces [see Figs. 6(f)–6(h)], similarly to other systems of four coupled resonators [66].

It should be mentioned, however, that the spectral positions of the resonances do not fully correspond to the eigenfrequencies. This happens because the system is

characterized by four eigenmodes with rather large imaginary parts, which means that the corresponding spectral widths of the resonances are also large and they may overlap. In particular, not only quasi-BIC but also a symmetric mode contribute to the observed resonances. This is also the reason why the resonance with $R_{f_2} \gg R_{f_1}$ looks to be slightly deformed, as an increase of R_{f_2} results in the interaction between the symmetric and antisymmetric modes. A comprehensive analysis of eigenmodes and EPs lies beyond the scope of this work, the aim of which is to develop a simply tunable meta-atom, which allows control of the quasi-BIC.

IV. CONCLUSION

In this work, coupling regimes of 2D Helmholtz resonators were investigated. It was shown that quasi-BIC and EP could be easily achieved by tuning the geometric parameters and intrinsic losses of the resonators. Experimental demonstrations reveal the resonant enhancement of absorption associated with quasi-BIC. The obtained results aim to extend the possibilities for the physics-based design of metamaterials and pave the route towards next-era devices for the efficient control of acoustic fields at the subwavelength scales.

ACKNOWLEDGMENTS

M. Krasikova, S.K., and A.B. acknowledge support from the BASIS foundation. A.B. acknowledges support from the Priority 2030 Federal Academic Leadership Program and the Russian Science Foundation (Project No. 22-42-04420). T.Y. acknowledges support from a European Union's Horizon Europe research and innovation program fellowship under Marie Skłodowska-Curie Grant Agreement No. 101063867.

M. Krasikova, M. Kuzmin, F.K., M.M., and T.Y. performed the experimental measurements, M. Krasikova, S.K. and F.K. provided numerical calculations. S.K. and M. Krasikova suggested the idea and developed the concept of the work. A.M., M.M., S.M., and A.B. supervised the project. All authors contributed to writing and editing of the manuscript.

The authors declare no competing interests.

[1] Michael E. McIntyre, Robert T. Schumacher Schumacher, and Jim Woodhouse, On the oscillations of musical instruments, J. Acoust. Soc. Am. **74**, 1325 (1983).

[2] Robert G. Arns and Bret E. Crawford, Resonant cavities in the history of architectural acoustics, Technol. Cult. **36**, 104 (1995).

[3] Joe Wolfe, Maëva Garnier, and John Smith, Vocal tract resonances in speech, singing, and playing musical instruments, HFSP J. **3**, 6 (2009).

[4] Ross M. Henderson, in *Medical Imaging 1997: Physics of Medical Imaging* (SPIE, Newport Beach, CA, United States, 1997), Vol. 3032, p. 142.

[5] Lennart D. Johns, Nonthermal effects of therapeutic ultrasound: The frequency resonance hypothesis, J. Athl. Train. **37**, 293 (2002).

[6] Kerstin Länge, Bastian E. Rapp, and Michael Rapp, Surface acoustic wave biosensors: A review, Anal. Bioanal. Chem. **391**, 1509 (2008).

[7] Robert G. Leisure and Frank A. Willis, Resonant ultrasound spectroscopy, J. Phys.: Condens. Matter **9**, 6001 (1997).

[8] Ming Yuan, Ziping Cao, Jun Luo, and Xiujian Chou, Recent developments of acoustic energy harvesting: A review, Micromachines **10**, 48 (2019).

[9] C. Aerts, Probing the interior physics of stars through asteroseismology, Rev. Mod. Phys. **93**, 015001 (2021).

[10] Steven A. Cummer, Johan Christensen, and Andrea Alù, Controlling sound with acoustic metamaterials, Nat. Rev. Mater. **1**, 1 (2016).

[11] Guancong Ma and Ping Sheng, Acoustic metamaterials: From local resonances to broad horizons, Sci. Adv. **2**, e1501595 (2016).

[12] Badreddine Assouar, Bin Liang, Ying Wu, Yong Li, Jian-Chun Cheng, and Yun Jing, Acoustic metasurfaces, Nat. Rev. Mater. **3**, 460 (2018).

[13] Sam Hyeon Lee, Choon Mahn Park, Yong Mun Seo, Zhi Guo Wang, and Chul Koo Kim, Acoustic metamaterial with negative density, Phys. Lett. A **373**, 4464 (2009).

[14] Jensen Li and C. T. Chan, Double-negative acoustic metamaterial, Phys. Rev. E **70**, 055602 (2004).

[15] Jensen Li, Lee Fok, Xiaobo Yin, Guy Bartal, and Xiang Zhang, Experimental demonstration of an acoustic magnifying hyperlens, Nat. Mater. **8**, 931 (2009).

[16] Yong Li and Badreddine M. Assouar, Acoustic metasurface-based perfect absorber with deep subwavelength thickness, Appl. Phys. Lett. **108**, 063502 (2016).

[17] Haoran Xue, Yihao Yang, and Baile Zhang, Topological acoustics, Nat. Rev. Mater. **7**, 974 (2022).

[18] Xiujuan Zhang, Farzad Zangeneh-Nejad, Ze-Guo Chen, Ming-Hui Lu, and Johan Christensen, A second wave of topological phenomena in photonics and acoustics, Nature **618**, 687 (2023).

[19] Xu Wang, Ruizhi Dong, Yong Li, and Yun Jing, Non-local and non-Hermitian acoustic metasurfaces, Rep. Prog. Phys. **86**, 116501 (2023).

[20] Hussein Nassar, Behrooz Yousefzadeh, Romain Fleury, Massimo Ruzzene, Andrea Alù, Chiara Daraio, Andrew N. Norris, Guoliang Huang, and Michael R. Haberman, Nonreciprocity in acoustic and elastic materials, Nat. Rev. Mater. **5**, 667 (2020).

[21] Chia Wei Hsu, Bo Zhen, A. Douglas Stone, John D. Joannopoulos, and Marin Soljačić, Bound states in the continuum, Nat. Rev. Mater. **1**, 1 (2016).

[22] Kirill L. Koshelev, Zarina F. Sadrieva, Alexey A. Shcherbakov, Yu.S. Kivshar, and Andrey A. Bogdanov, Bound states in the continuum in photonic structures, Phys.-Usp. **66**, 494 (2023).

[23] John von Neumann and Eugene. P. Wigner, in *The Collected Works of Eugene Paul Wigner: Part A: The Scientific Papers, The Collected Works of Eugene Paul Wigner*,

edited by Arthur S. Wightman (Springer, Berlin, Heidelberg, 1993), p. 291.

[24] Zhuangzhuang Li, Jien Wu, Xueqin Huang, Jiuyang Lu, Feng Li, Weiyin Deng, and Zhengyou Liu, Bound state in the continuum in topological inductor–capacitor circuit, Appl. Phys. Lett. **116**, 263501 (2020).

[25] Meng Kang, Tao Liu, C. T. Chan, and Meng Xiao, Applications of bound states in the continuum in photonics, Nat. Rev. Phys. **5**, 659 (2023).

[26] Almas F. Sadreev, Interference traps waves in an open system: Bound states in the continuum, Rep. Prog. Phys. **84**, 055901 (2021).

[27] Sibo Huang, Tuo Liu, Zhiling Zhou, Xu Wang, Jie Zhu, and Yong Li, Extreme sound confinement from quasibound states in the continuum, Phys. Rev. Appl. **14**, 021001 (2020).

[28] Ilya Deriy, Ivan Toftul, Mihail Petrov, and Andrey Bogdanov, Bound states in the continuum in compact acoustic resonators, Phys. Rev. Lett. **128**, 084301 (2022).

[29] Sibo Huang, Shuhuan Xie, He Gao, Tong Hao, Shuang Zhang, Tuo Liu, Yong Li, and Jie Zhu, Acoustic Purcell effect induced by quasibound state in the continuum, Fundam. Res. **4**, 57 (2024).

[30] Liyun Cao, Yifan Zhu, Sheng Wan, Yi Zeng, Yong Li, and Badreddine Assouar, Perfect absorption of flexural waves induced by bound state in the continuum, Extreme Mech. Lett. **47**, 101364 (2021).

[31] Haiyan Zhang, Shanshan Liu, Zhiwei Guo, Shengyu Hu, Yuguang Chen, Yunhui Li, Yong Li, and Hong Chen, Topological bound state in the continuum induced unidirectional acoustic perfect absorption, Sci. China Phys., Mech. Astron. **66**, 284311 (2023).

[32] Stefan Hein and Werner Koch, Acoustic resonances and trapped modes in pipes and tunnels, J. Fluid Mech. **605**, 401 (2008).

[33] Stefan Hein, Werner Koch, and Lothar Nannen, Trapped modes and Fano resonances in two-dimensional acoustical duct–cavity systems, J. Fluid Mech. **692**, 257 (2012).

[34] A. A. Lyapina, D. N. Maksimov, A. S. Pilipchuk, and A. F. Sadreev, Bound states in the continuum in open acoustic resonators, J. Fluid Mech. **780**, 370 (2015).

[35] Lujun Huang, Yan Kei Chiang, Sibo Huang, Chen Shen, Fu Deng, Yi Cheng, Bin Jia, Yong Li, David A. Powell, and Andrey E. Miroshnichenko, Sound trapping in an open resonator, Nat. Commun. **12**, 4819 (2021).

[36] Lujun Huang, Bin Jia, Yan Kei Chiang, Sibo Huang, Chen Shen, Fu Deng, Tianzhi Yang, David A. Powell, Yong Li, and Andrey E. Miroshnichenko, Topological supercavity resonances in the finite system, Adv. Sci. **9**, 2200257 (2022).

[37] Lujun Huang, Bin Jia, Artem S. Pilipchuk, Yankei Chiang, Sibo Huang, Junfei Li, Chen Shen, Evgeny N. Bulgakov, Fu Deng, David A. Powell, Steven A. Cummer, Yong Li, Almas F. Sadreev, and Andrey E. Miroshnichenko, General framework of bound states in the continuum in an open acoustic resonator, Phys. Rev. Appl. **18**, 054021 (2022).

[38] Omer Haq and Sergei Shabanov, Bound states in the continuum in elasticity, Wave Motion **103**, 102718 (2021).

[39] Liyun Cao, Yifan Zhu, Yanlong Xu, Shi-Wang Fan, Zhichun Yang, and Badreddine Assouar, Elastic bound state in the continuum with perfect mode conversion, J. Mech. Phys. Solids **154**, 104502 (2021).

[40] Dongwoo Lee, Jeonghoon Park, Seokwoo Kim, Jungho Mun, Jaekyung Kim, Xianji Piao, Namkyoo Park, and Junsuk Rho, Elastic bound states in the continuum by acoustoelastic interaction, Extreme Mech. Lett. **61**, 101965 (2023).

[41] Shuowei An, Tuo Liu, Liyun Cao, Zhongming Gu, Haiyan Fan, Yi Zeng, Li Cheng, Jie Zhu, and Badreddine Assouar, Multibranch elastic bound states in the continuum, Phys. Rev. Lett. **132**, 187202 (2024).

[42] Kirill Koshelev, Sergey Lepeshov, Mingkai Liu, Andrey Bogdanov, and Yuri Kivshar, Asymmetric metasurfaces with high-Q resonances governed by bound states in the continuum, Phys. Rev. Lett. **121**, 193903 (2018).

[43] Viktar S. Asadchy, Ana Díaz-Rubio, and Sergei A. Tretyakov, Bianisotropic metasurfaces: Physics and applications, Nanophotonics **7**, 1069 (2018).

[44] Steven R. Craig, Xiaoshi Su, Andrew Norris, and Chengzhi Shi, Experimental realization of acoustic bianisotropic gratings, Phys. Rev. Appl. **11**, 061002 (2019).

[45] Anton Melnikov, Yan Kei Chiang, Li Quan, Sebastian Oberst, Andrea Alù, Steffen Marburg, and David Powell, Acoustic meta-atom with experimentally verified maximum Willis coupling, Nat. Commun. **10**, 3148 (2019).

[46] Junfei Li, Ailing Song, and Steven A. Cummer, Bianisotropic acoustic metasurface for surface-wave-enhanced wavefront transformation, Phys. Rev. Appl. **14**, 044012 (2020).

[47] Anton Melnikov, Sören Köble, Severin Schweiger, Yan Kei Chiang, Steffen Marburg, and David A. Powell, Microacoustic metagratings at ultra-high frequencies fabricated by two-photon lithography, Adv. Sci. **9**, 2200990 (2022).

[48] Yuto Ashida, Zongping Gong, and Masahito Ueda, Non-Hermitian physics, Adv. Phys. **69**, 249 (2020).

[49] Walter D. Heiss, The physics of exceptional points, J. Phys. A: Math. Theor. **45**, 444016 (2012).

[50] Ş. K. Özdemir, S. Rotter, F. Nori, and L. Yang, Parity–time symmetry and exceptional points in photonics, Nat. Mater. **18**, 783 (2019).

[51] Vladimir Igoshin, Mariia Tsimokha, Anastasia Nikitina, Mihail Petrov, Ivan Toftul, and Kristina Frizyuk, Exceptional points in single open acoustic resonator due to symmetry breaking, Phys. Rev. B **109**, 144102 (2024).

[52] Mohammad-Ali Miri and Andrea Alù, Exceptional points in optics and photonics, Science **363**, eaar7709 (2019).

[53] Chen Shen, Junfei Li, Xiuyuan Peng, and Steven A. Cummer, Synthetic exceptional points and unidirectional zero reflection in non-Hermitian acoustic systems, Phys. Rev. Mater. **2**, 125203 (2018).

[54] Claire Bourquard and Nicolas Noiray, Stabilization of acoustic modes using Helmholtz and quarter-wave resonators tuned at exceptional points, J. Sound Vib. **445**, 288 (2019).

[55] Vassos Achilleos, Georgios Theocharis, Olivier Richoux, and Vincent Pagneux, Non-Hermitian acoustic metamaterials: Role of exceptional points in sound absorption, Phys. Rev. B **95**, 144303 (2017).

[56] Anton Melnikov, Marcus Maeder, Niklas Friedrich, Yan Pozhanka, Alexander Wollmann, Michael Scheffler, Sebastian Oberst, David Powell, and Steffen Marburg,

Acoustic metamaterial capsule for reduction of stage machinery noise, J. Acoust. Soc. Am. **147**, 1491 (2020).

[57] Felix Kronowetter, Lisa Pretsch, Yan Kei Chiang, Anton Melnikov, Shahrokh Sepehrirahnama, Sebastian Oberst, David A. Powell, and Steffen Marburg, Sound attenuation enhancement of acoustic meta-atoms via coupling, J. Acoust. Soc. Am. **154**, 842 (2023).

[58] Mariia Krasikova, Sergey Krasikov, Anton Melnikov, Yuri Baloshin, Steffen Marburg, David A. Powell, and Andrey Bogdanov, Metahouse: Noise-insulating chamber based on periodic structures, Adv. Mater. Technol. **8**, 2200711 (2023).

[59] Mariia Krasikova, Aleksandra Pavliuk, Sergey Krasikov, Mikhail Kuzmin, Andrey Lutovinov, Anton Melnikov, Yuri Baloshin, David A. Powell, Steffen Marburg, and Andrey Bogdanov, Broadband noise-insulating periodic structures made of coupled Helmholtz resonators, APL Mater. **12**, 011115 (2024).

[60] Alan R. Selfridge, Approximate material properties in isotropic materials, IEEE Trans. Son. Ultrason. **32**, 381 (1985).

[61] in Vol. 143 of *Topics in Applied Physics*, edited by Noé Jiménez, Olga Umnova, and Jean-Philippe Groby (Springer International Publishing, Cham, 2021).

[62] See the Supplemental Material at http://link.aps.org/supplemental/10.1103/PhysRevApplied.22.024045, which includes Refs. [67–70], for additional information on experimental measurements and numerical calculations, including the results of the asymmetric absorption induced by the inversion-symmetry breaking and brief estimation of the applicability of the considered system for gas sensing. In addition, the Supplemental Material contains the lumped-element model, allowing us to semianalytically describe the system in terms of the mutual impedance of the resonators.

[63] Felix Kronowetter, Marcus Maeder, Yan Kei Chiang, Lujun Huang, Johannes D. Schmid, Sebastian Oberst, David A. Powell, and Steffen Marburg, Realistic prediction and engineering of high-Q modes to implement stable Fano resonances in acoustic devices, Nat. Commun. **14**, 6847 (2023).

[64] Haoye Qin, Xiaodong Shi, and Haiyan Ou, Exceptional points at bound states in the continuum in photonic integrated circuits, Nanophotonics **11**, 4909 (2022).

[65] Kun Ding, Guancong Ma, Meng Xiao, Z. Q. Zhang, and C. T. Chan, Emergence, coalescence, and topological properties of multiple exceptional points and their experimental realization, Phys. Rev. X **6**, 021007 (2016).

[66] Yiwei Peng, Yumeng Yang, Hongsheng Chen, Yuanzhen Li, and Fei Gao, Regulation of multiple exceptional points in a plasmonic quadrumer, Opt. Mater. Express **14**, 1475 (2024).

[67] Torbjörn A. Johansson and Mendel Kleiner, Theory and experiments on the coupling of two Helmholtz resonators, J. Acoust. Soc. Am. **110**, 1315 (2001).

[68] Michael J. A. Smith, Philip A. Cotterill, David Nigro, William J. Parnell, and Ian D. Abrahams, Asymptotics of the meta-atom: Plane wave scattering by a single Helmholtz resonator, Philos. Trans. R. Soc. A: Math., Phys. Eng. Sci. **380**, 20210383 (2022).

[69] Haleh Nazemi, Aashish Joseph, Jaewoo Park, and Arezoo Emadi, Advanced micro- and nano-gas sensor technology: A review, Sensors **19**, 1285 (2019).

[70] Hatice Altug, Sang-Hyun Oh, Stefan A. Maier, and Jiří Homola, Advances and applications of nanophotonic biosensors, Nat. Nanotechnol. **17**, 5 (2022).